fertile source for the high-Ti basalt (CaO/TiO_2 : 10–4; Al_2O_3/TiO_2 : 18–8)[1]. Assuming a similar source, our dataset[2] indicates that the low-Ti basalt (CaO/TiO_2 : 18–8; Al_2O_3/TiO_2 : 26–18) has formed by relatively higher degrees of partial melting than the high-Ti basalt. However, other datasets[3–5] clearly indicate that the source of the low-Ti basalt was relatively depleted (Cao/TiO_2 : 35–10; Al_2O_3/TiO_2 : 45–15). The low-Ti basalt was probably formed by remelting of a source which had undergone a previous episode of magma extraction[1]. Therefore, Figure 2 of our paper clearly indicates heterogeneity in the mantle source of the basalts which is also evident from their REE patterns (Figure 3). The two cross-cutting REE patterns cannot be obtained by different degrees of partial melting of a homogeneous source[6]. The HREE and Ti depletion in the low-Ti basalt can be due to the following reasons:

i) The low-Ti basalt was formed by relatively higher degrees of partial melting. ii) Mantle wedge of the low-Ti basalt has undergone previous episodes of magma extraction. iii) Mantle residue of the low-Ti basalt has higher proportions of garnet[7] and/or rutile[8].

The LREE enrichment in the low-Ti basalt clearly indicates higher subduction fluxes which is also evident from higher LILE contents in this basalt[9–11]. Pandey has stated that CaO content in the low-Ti basalt is more than high-Ti basalt, but from Table 1 it is evident that CaO content in the low-Ti basalt (7.08 wt%) is less than that in high-Ti basalt (8.50 wt%). Lower concentration of CaO in the low-Ti basalt probably indicates plagioclase fractionation which is also evident from negative Eu-anomaly shown by this basalt.

2. Derivation of arc-related magmas is not possible by thermal plumes or crustal underplating. Arc-related magmas are generated by decompression melting in the mantle wedge, augmented by aqueous fluids derived from the subducting oceanic crust[7,9,12–14].

3. Both the basaltic suites have high MgO-content (12–7 wt%) which rules out the possibility of their crustal contamination[15–17]. $MgO > 6$ wt% is generally considered as an adequate filter for AFC processes[15]. Therefore, we have not correlated the two suites by AFC. We have put a question mark for LILE because these are potentially mobile elements in altered volcanics such as Khairagarh basalts[18]. Therefore, LILE contents assume no importance in deciphering degrees of partial melting in these basalts. On the other hand, in altered and low grade volcanics, relatively immobile elements such as HFSE and REE assume vital importance in understanding degrees of partial melting and fractional crystallization[18]. LILE enrichment in the primitive arc-related magmas clearly indicates enrichment of the mantle wedge by subducting oceanic crust-derived fluids. Therefore, convergent margins are the zones of crust–mantle recycling.

1. Sun, S. S. and Nesbitt, R. W., *Geology*, 1978, **6**, 689–693.
2. Asthana, D., Dash, M. R., Pophare, A. M. and Khare, S. K., *Curr. Sci.*, 1996, **71**, 304–306.
3. Neogi, S., Miura, H. and Hariya, Y., *Precambr. Res.*, 1996, **76**, 77–91.
4. Deshmukh, G. G., Mohabey, N. K. and Deshpande, M. S., *Geol. Surv. India Spl. Publ. No. 28*, 1990, 260–286.
5. Sarkar, S. N., *Indian J. Earth Sci.*, 1994, **21**, 117–126.
6. Hanson, G. N., in *Geochemistry and Mineralogy of Rare Earth Elements* (eds Lipin, B. R. and McKay, G. A.), Mineral Soc. Am., 1989, vol. 21, pp. 79–97.
7. Hawkesworth, C. J., Gallagher, K., Hergt, J. M. and McDermott, F., *Lithos*, 1994, **33**, 169–188.
8. Brenan, J. M., Shaw, H. F., Phinney, D. L. and Ryerson, F. J., *Earth Planet. Sci. Lett.*, 1994, **128**, 327–339.
9. Pearce, J. A. and Parkinson, I. J., in *Magmatism and Plate Tectonics* (eds Pricard, H. M., Alabaster, T., Harris, N. B. W. and Neary, C. R.), Geol. Soc. Spl. Publ. No. 76, 1993, pp. 373–403.
10. Pearce, J. A. and Peate, D. W., *Annu. Rev. Earth Planet. Sci.*, 1995, **23**, 251–285.
11. Pearce, J. A., Baker, P. E., Harvey, P. K. and Luff, I. W., *J. Petrol.*, 1995, **36**, 1073–1109.
12. Arculus, R. J., *Lithos*, 1994, **33**, 189–208.
13. Davies, J. H. and Stevenson, D. J., *J. Geophys. Res.*, 1992, **97**, 2037–2070.
14. Tatsumi, Y., Furukawa, Y. and Yamashita, S., *J. Geophys. Res.*, 1994, **99**, 22275–22283.
15. Thirlwall, M. F., Smith, T. E., Graham, A. M. and Theodorou, N., *J. Petrol.*, 1994, **35**, 819–838.
16. Feigenson, M. D. and Carr, M. I., *Contrib. Mineral. Petrol.*, 1993, **113**, 226–235.
17. Carr, M. J., Feigenson, M. D. and Bennett, E. A., *Contrib. Mineral. Petrol.*, 1990, **105**, 369–380.
18. Stern, R. A., Syme, E. C., Bailes, A. H. and Lucas, S. B., *Contrib. Mineral. Petrol.*, 1995, **119**, 117–141.

D. ASTHANA
M. R. DASH
A. M. POPHARE
S. K. KHARE

Department of Applied Geology,
Indian School of Mines,
Dhanbad 826 004, India

Predicting monsoon rainfall and pressure indices from sea surface temperature

Several prediction techniques have been developed[1] to forecast the all India summer monsoon rainfall during the period, June–September. Among them, DWPJ-A, BMBPA-J and A-MR500 are found to be the most useful predictors. Nicholls[2] reported that the SST in the north Australia–Indonesian region (5–15°S, 120–160°E) is useful to predict monsoon rainfall.

Several studies[3–6] reported the relationship between SST in Indian ocean and monsoon rainfall over the Indian subcontinent. But, there is a divergent opinion on this aspect which is partly attributed to the poor quality of SST data in the Indian ocean[7]. Using the latest and high quality data set[8] on SST anomalies (MOHSST.6), an attempt is made here to re-examine the role of Indian Ocean SST in monsoon rainfall.

Data on SST anomalies (SSTA) in the grid, 0–5°N, 80–85°E, for the period, 1967–87 and three different rainfall series (R_1, All India monsoon rainfall (1847–1990) in mm based on arithmetic average of 16 representative stations[9]; R_2, arithmetic average of monsoon rainfall of 32 representative stations[10]; and R_3, rainfall anomalies[11] in cm) have been used in the computations. Correlation coefficients between SSTA and (i) DWPJ-A, (ii) BMBPA-J and (iii) A-MR500, are also computed. Data on DWPJ-A, BMBPA-J and A-MR500 are taken from the earlier studies[9,12,13].

Correlations have been computed with (– 1) year and (0) year lags following the method given by Nicholls[2] (correlations of 0.45 are significant at 95% level). The results are shown in Figure 1.

All India summer monsoon rainfall (R_1, R_2 and R_3) is strongly and positively correlated ($r = 0.75$) with the SSTA in the grid, 0–5°N; 80–85°E during October and November months of the previous year. SSTA in February (0 year) is also well correlated with R_1 (Figure 1 *a*). Negative and strong correlation is noticed between R_1, R_3 and SSTA in November, after the withdrawal of monsoon. This could be due to the advection of heat from west to east through equatorial jet which appears in October–November. The jet deepens the mixed layer depth towards east. This may distribute the heat to deeper depth and results in changes in SST anomalies[14].

SSTA in November (– 1 year) is strongly and negatively correlated (– 0.74) with DWPJ-A (Figure 1 *d*) while BMBPA-J is significantly and positively correlated (0.75) with the SSTA during November and December (Figure 1 *e*). A-MR500 is positively and significantly correlated (0.63) with the SSTA in October (– 1 year) (Figure 1 *f*).

To identify the changes in the correlations with time, sliding window correlations have been computed with a width of 26 years, from 1950 to 1991. Table 1 shows the sliding window correlations between SST and (a) monsoon rainfall (R_2), and (b) pressure indices (DWPJ-A, BMBPA-J). Correlations between April SST in the north Australia–Indonesian region (5–15°S; 120–160°E) and monsoon rainfall (R_2) are also shown in column (d) in Table 1. Correlation between October SST in the grid, 0–5°N; 80–85°E, and monsoon rainfall is significant from 1960 onwards. A similar feature is noticed between November SST (– 1 year) and DWPJ-A. But, BMBPA-J is significantly and positively correlated from 1953 onwards. All the correlations (columns a, b, c) show an increasing trend since 1950 onwards. A similar feature was also reported[1] earlier. The correlation between April SST in the north Australia–Indonesian region and monsoon rainfall (R_2) is significant and consistent throughout the study period and a decreasing trend is noticed in the recent period, 1966–91. It is interesting to see that the correlation during the above period is increased in the case of Indian ocean SST and R_2. This may be due to the warming of eastern equatorial Indian Ocean during the recent decades or due to the strong coupling between ocean–land–atmosphere system during the recent period compared with the earlier period as conjectured by Krishnakumar *et al.*[1]. The correlation between Indian monsoon rainfall and April SST in the north Australia–Indonesian region is found to be 0.55 (ref. 2) for the period, 1950–91. The correlation coefficient between October SST of the previous year in the grid, 0–5°N; 80–85°E and monsoon rainfall for the entire period is 0.40 which is statistically significant at 95% level.

From the overall results, it can be concluded that SSTA during October and November months in the EEIO is useful to predict monsoon rainfall and pressure indices. I am not aware of any earlier study which has shown the relationship between SSTA and pressure indices. It is inferred that the eastward propagating low frequency convective systems (LFCs) which originate in the warm pool region in the equatorial Indian ocean[15] could be the main mechanism behind the relationship of SSTA with different parameters discussed above. Secondly, the SST anomalies in this region can affect the 'walker circulation'[11], which is reflected in the strong correlations noticed between SST and (i) DWPJ-A, and (ii) BMBPA-J. Since the 500 mb ridge location along 75°E before monsoon is controlled by

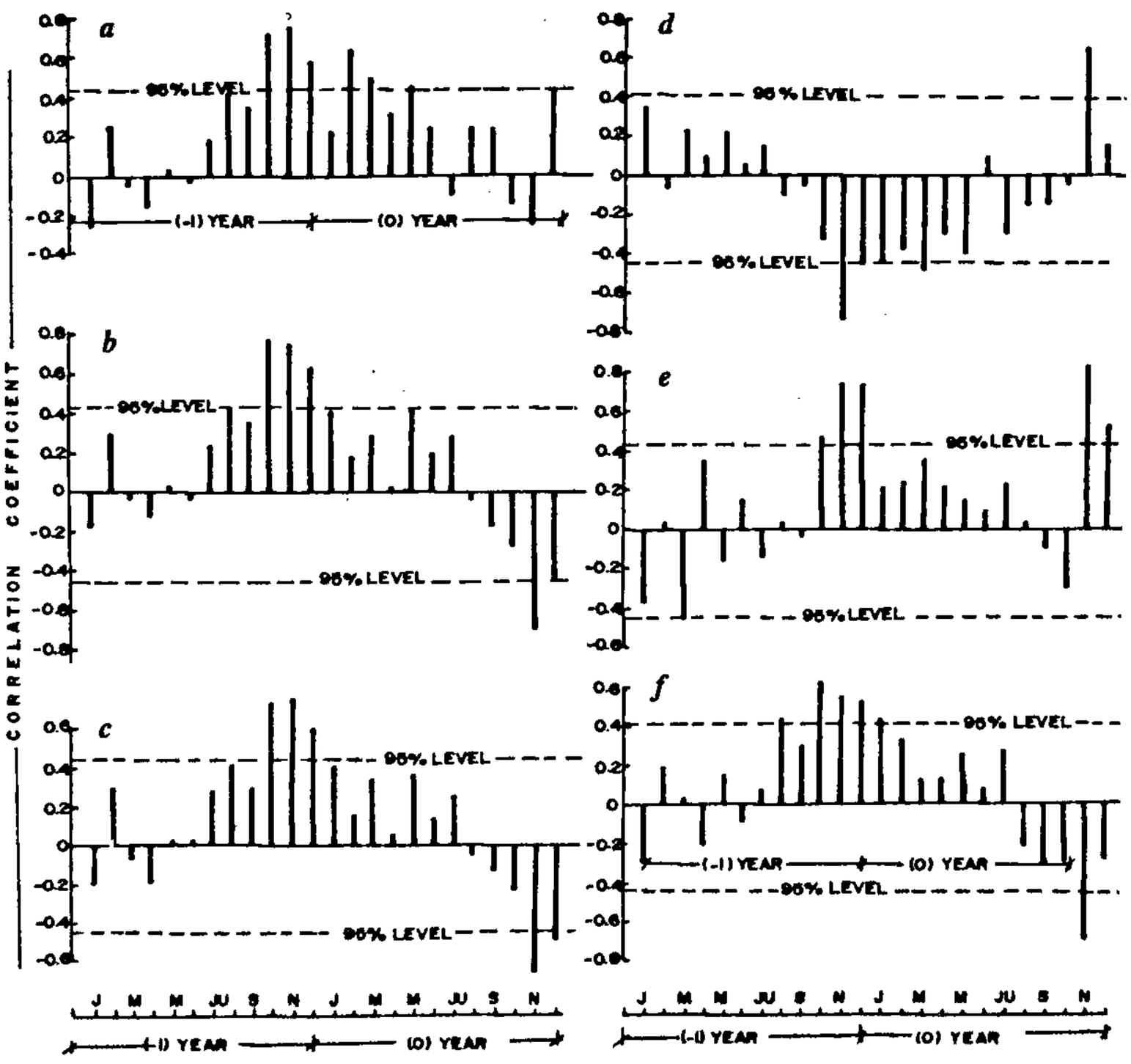

Figure 1. Correlation coefficients between SST and (*a*) R_1, (*b*) R_2, (*c*) R_3, (*d*) DWPJ-A, (*e*), BMBPA-J and (*f*) A-MR500.

Table 1. Sliding window correlation between SST and different parameters

Period	(a)	(b)	(c)	(d)
1950–75	0.11	−0.20	0.26	0.51
1951–76	0.11	−0.26	0.31	0.50
1952–77	0.09	−0.26	0.35	0.46
1953–78	0.14	−0.30	0.40	0.47
1954–79	0.15	−0.31	0.41	0.45
1955–80	0.15	−0.30	0.41	0.45
1956–81	0.15	−0.37	0.43	0.55
1957–82	0.22	−0.38	0.64	0.53
1958–83	0.35	−0.51	0.58	0.55
1959–84	0.33	−0.53	0.58	0.54
1960–85	0.35	−0.59	0.64	0.51
1961–86	0.40	−0.58	0.65	0.50
1962–87	0.57	−0.66	0.66	0.50
1963–88	0.63	−0.67	0.65	0.53
1964–89	0.65	−0.67	0.65	0.53
1965–90	0.64	−0.67	0.66	0.54
1966–91	0.67	−0.65	–	0.47

(a) Correlation between October SST of the previous year in 0–5°N; 80–85°E and R_2.
(b) Correlation between November SST of the previous year in the same area and DWPJ-A.
(c) Correlation between November SST of the previous year in the above area and BMBPA-J.
(d) Correlation between April SST in the north Australia–Indonesia region (5–15°S; 120–160°E) and R_2.

the slowly varying planetary circulation and SST anomalies in the equatorial region[11] the observed relationship between October SSTA and A-MR500 is justified. More northward (southward) displacement of the 500 mb ridge position is a precursor for strong (weak) monsoon. In view of the above discussion, the observed strong correlation between October and November SSTA (– 1 year) and monsoon rainfall appears to be reasonable.

It is suggested that the SST in the EEIO may be included in the operational forecast model of India Meteorological Department.

1. Krishnakumar, K., Soman, M. K. and Rupakumar, K., *Weather*, 1995, **50**, 449–467.
2. Nicholls, N., *J. Clim.*, 1995, **8**, 1463–67.
3. Rao Kusuma, G. and Goswami, B. N., *Mon. Wea. Rev.*, 1985, **116**, 558–568.
4. Sadhuram, Y., Ramesh Babu, V., Gopalakrishna, V. V. and Sarma, M. S. S., *Indian J. Mar. Sci.*, 1991, **20**, 106–109.
5. Varma, R. K., *Mausam*, 1994, **45**, 205–212.
6. Joseph, P. V. and Pillai, P. V., *Mausam*, 1984, **35**, 323–330.
7. Terray, P., *J. Met. Soc. Japan*, 1994, **72**, 359–386.
8. Parker, D. E., Personal communication, 1996.
9. Parthasarathy, B., Rupakumar, K. and Munot, A. A., *J. Climate*, 1992, **5**, 979–986.
10. Sontekke, N. N., Pant, G. B. and Singh, N., *J. Climate*, 1993, **6**, 1807–1811.
11. Webster, P. J. and Yang, S., *Q. J. R. Meteorol. Soc.*, 1992, **118**, 877–926.
12. Weare, B. C., *J. Atmos. Sci.*, 1984, **36**, 2279–91.
13. Krishnakumar, K., Rupakumar, K. and Pant, G. B., *J. Climate*, 1992, **5**, 979–986.
14. Hastenrath, S. and Grieschar, L. L., *Climatic Atlas of the Indian Ocean. Part III, Upper Ocean Structure*, Univ. of Wisconsin Press, 1989.
15. Zhu, B. and Wang, B., *J. Atmos. Sci.*, 1993, **50**, 184–199.

ACKNOWLEDGEMENTS. This work was done at the Department of Oceanography, University of Southampton, Southampton Oceanography Centre, Southampton, UK, under TCTP fellowship offered by the British Council, Manchester.

Y. SADHURAM

National Institute of Oceanography, Regional Centre, 176, Lawsons Bay Colony, Visakhapatnam 530 017, India

On the age and fauna of beachrock of Kegaon Coast, Uran, Maharashtra

Outcrops of beachrock occur as isolated patches all along the coast of Maharashtra and comprise conglomerates, shell limestone bands and consolidated dune sand designated as 'karal'. The karal has been dated and found to range from Middle to Late Holocene in age[1–4]. The beachrock of Kegaon Coast of Uran forms the northernmost outcrop of the Raigad district. We aim to comment here on the age and paleoenvironment of the karal of Uran. It is well exposed in the intertidal and supratidal zone, stretching over 500 m and resting on highly fractured and well-jointed amygdular basalt. The karal has an uneven contact with basalt and exhibits varying thickness (Figure 1). The lithologic section studied shows development of approximately 3.5 m thick sediments with a basal conglomeritic zone followed by laminated shell limestone bands and dune sand (Figure 2).

Survey using theodolite was carried out at a location (18°52′58″N and 72°54′48″E) to determine the position of the beachrock with respect to the present MSL (Figure 3). The bases of conglomerate and dune sand lie at 1.5 m and 2.5 m above MSL respectively. However, the thickness of the beachrock varies from place to place. A section at Uran (18°50′25″N and 72°50′50″E) illustrated by Agarwal and Guzder[1] appears to be 4 m thick, while Kale *et al.*[5] gave a range of thickness from 1.5 m to 2 m for the beachrock and 0.9 m to 1.5 m for the dune sand exposed at a location having coordinates 18°52′30″N and 72°54′56″E.

The beachrock is compact, fairly well consolidated towards the bottom and fragile towards the top. The fauna recovered from the beachrock comprises mollusca, foraminifera, broken fragments of bryozoa, corals, etc. The shell limestone in particular, is rich in gastropods species,